NUMERICAL LINEAR ALGEBRA WITH APPLICATIONS
Numer. Linear Algebra Appl. 2000; **00**:1–6 *Prepared using* nlaauth.cls *[Version: 2002/09/18 v1.02]*

Two multigrid algorithms for an inverse problem in Electrical Impedance Tomopraphy

R. Gandlin*, A. Brandt*

Department of Computer Science and Applied Mathematics,
Weizmann Institute of Science, Rehovot, 76100, ISRAEL

SUMMARY

The subject of this paper is an application of the multigrid method to the inverse problem in the Electrical Impedance Tomography. The multigrid algorithm of a new type has been developed for solving this problem, involving near-boundary semi-coarsening cycles within full-coarsening cycles. The results of the developed algorithm were compared with another previously developed multigrid algorithm which uses the classical regularization technique. Both algorithm give nearly the same accuracy, but the new algorithm is much cheaper since it does not have all the artificial parameters as the algorithm with classical regularization does.

KEY WORDS: impedance tomography, multigrid, regularization.

INTRODUCTION

Many partial-differential problems in the real world do not arise as fully well-posed mathematical equations. The partial-differential equations (PDE's) and their boundary and initial conditions are often only partly or approximately known, and instead of full knowledge, a set of observational data is supplied. The data are usually noisy and do not stably determine a unique solution. Examples include ground-water flows where permeability is only partly known; global atmospheric and oceanic circulation and weather prediction; non-destructive analysis of materials; optimal control problems; various devices of medical imaging; surface reconstruction in computer graphics and computer-aided design; and so on.

Multigrid methods are known to provide the most efficient solvers to many well-posed boundary-value PDE problems. In the case of ill-determined problems they can provide several additional advantages. Unlike evolution problems with well-posed initial conditions which can be solved by direct marching in time, when only scattered data are known, each datum affects both earlier and later solution values, so simple marching cannot be used, and fast solvers would again require multigrid methods. Also, multiscale formulations provide ill-posed problems with

*Correspondence to: rima@wisdom.weizmann.ac.il, achi@wisdom.weizmann.ac.il

additional tools, including: one-shot solution of non-linearities; local refinement techniques; space+time parallel processing; unlimited correlation ranges and efficient representation of direct and inverse covariance matrices; multiscale organization of the observational data and in particular coarse-scale representation of oscillatory data; etc. Multigrid solvers can provide natural regularization to many ill-posed problems, since the main ill-posedness in those problems is the long term and long range influence of fine-scale oscillations, while the multiscale large-scale interactions are mediated by coarse grids that omit those oscillations.

The main goal of this research has therefore been to develop multigrid techniques suitable for typical inverse problems. A basic difficulty is that the required multigrid solvers for such problems cannot follow familiar standard multigrid algorithms. We chose the inverse problem for electrical impedance tomography since it is a representative and important example. Motivated by medical-imaging and non-destructive-material and ground-permeability analysis devices, this is a stationary diffusion problem, where the diffusion coefficient at each point is unknown while solution and solution-derivative values are given, mostly on the boundary.

For this problem two multigrid algorithms were developed, one uses the classical regularizaton technique, the other uses natural multi-scale regularization. Second algorithm is a new type of a multigrid algorithm which has been developed for solving the problem, involving near-boundary semi-coarsening cycles within full-coarsening cycles. Both algorithms give nearly the same accuracy, but the second algorithm is much cheaper since it does not have all those artificial parameters as the first algorithm does. Here we report the second algorithm in details while first algorithm with classical regularization just briefly mentioned. For more details see [11].

The work for solving the inverse problem is proportional to the number of points *near the boundary of measurements only*, while the work for solving the corresponding direct problem is proportional to the number of points *in the entire domain*. It demonstrates the following methodological point: ill-posedness of an inverse problem does not necessarily imply a more expensive solution process. On the contrary: once the nature of the ill-posedness has been generally understood, to solve an inverse problem may even be much less expensive than to solve the corresponding direct problem, since less information is in principle recoverable.

One of the most attractive features of EIT is the feasibility of continuously monitoring a process, provided that fast computational algorithms for delivering real-time images of the conductivity distributions are incorporated into an EIT device. Here we do not deal with the real EIT problem for medical use but with a mathematical model with many assumptions on one hand and neglecting other knowledge on the other. For instance, in the real EIT the range of conductivity values is known but we do not use this in our model. Another simplification is that the general EIT problem is to find an admittivity function $\gamma(x,\omega) = \sigma + i\omega\epsilon$ where σ is an electrical conductivity and ϵ is an electrical permittivity, while here we refer to the static case $\omega = 0$. The main goal was to investigate the difficulties from the mathematical point of view and then to develop tools to deal with those difficulties. The ideas developed here for efficient solving of this pure mathematical model can be now used as an integrated part of a real EIT solver.

The first description of the inverse EIT problem was given by Calderon [8]. Kohn and Vogelius [13] showed that under certain assumptions the conductivity of a medium is uniquely determined by the Neumann-to-Dirichlet mapping. Then Sylvester and Uhlmann [16] provided a general framework for proving uniqueness of the solution of the inverse problem. Alessandrini [2] gave a mathematical explanation for the blurriness of conductivity images and proved that

the conductivity depends on the EIT data in a very weak way. Therefore the inverse problem of EIT is ill-posed, and some regularization is necessary if conductivity is to be obtained stably from data.

Electrical impedance tomography has been studied extensively in the last two decades. Isaacson and Cheney [19] and Allers and Santosa [20] showed that the resolution of the images improves as the number of electrodes increases. Gisser, Isaacson and Newell [21] and Cherkaev, Tripp [22] discuss the question of optimal currents. Allers, Santosa [20], Barber, Brown [23], Cheney, Isaacson, Newell [24] investigated linearization algorithms for EIT. Engl, Hanke, Neubauer [25] concentrated on the question how to choose regularization parameter. There are some recent publication on multigrid reconstructions for EIT. McCormick, Wade [26] discussed multigrid method for linearized problem. Ascher, Haber [3] showed that the regularization parameter can be determined on the coarse grid and conductivity σ can then be imaged on a finer grid. Nonlinear multigrid is discussed in [27] and [17] by Borcea.

Fast multigrid algorithms for solving the inverse problem for two special cases of a constant conductivity and of a certain form of variable conductivity, were designed by F. Shmulyian [25]. In her work the ill-posed inverse problem of EIT is formulated, regularized by the Tikhonov regularization method and discretized. The practical aspects of designing the FMG solver and the results of the numerical experiments for the cases mentioned above are also reported in [25].

The outline of this paper is as follows:

In §1 the original inverse problem for EIT is described and some simplifications are introduced. In §2 the original ill-posed inverse problem for EIT is solved by multigrid algorithm that does not use any explicit regularization but regularizes itself by careful choice of grids. This reduces significantly the total work of this algorithm comparing with the algorithm with classical regularization [28]. Finally, some numerical results comparing two multigrid algorithms are reported in §3.

1. Problem statment

An EIT device for medical use consists of a set of electrodes attached to the chest of a patient. A small *known* current is passed between two driver electrodes. In each measurement a current is passed through a different electrode pair, while the voltage drops at *all* the electrodes are recorded. The collected data are used in order to compute the conductivity distribution in a part of the patient's chest and then to display it on a screen in order to detect anomalies, such as tumors.

The general EIT problem is to find an admittivity function $\gamma(x,\omega) = \sigma + i\omega\epsilon$ where σ is an electrical conductivity and ϵ is an electrical permittivity. Here we consider the static case $\omega = 0$.

If the domain being imaged is denoted by Ω, the voltage potential in Ω — by u and the electrical conductivity — by σ (positive function), then the Maxwell's equation of electromagnetics at zero-frequency ($\omega = 0$) is $\nabla \cdot [\sigma(\mathbf{x})\nabla u(\mathbf{x})] = 0, \quad \mathbf{x} = (x,y) \in \Omega$. The electrodes are assumed to generate a current flux density distribution on the boundary $\partial\Omega$ of Ω, which translates into a Neumann boundary condition: $(\sigma \frac{\partial u}{\partial \mathbf{n}})\Big|_{\partial\Omega} = g$, where the vector $\mathbf{n}$ is the outward unit normal to the domain Ω. The voltage potentials on the boundary $\partial\Omega$ are

measured and translated into a Dirichlet boundary condition: $u\big|_{\partial\Omega} = f$.

If N electrodes are attached to the boundary points $\partial x_1, \ldots, \partial x_N \in \partial\Omega$, the data gathered in a single measurement comprise a set of N real numbers $f_j = u(\partial \mathbf{x}_j)$, $j = 1, \ldots, N$. In a real EIT process, K different current flux densities g^k, $k = 1, \ldots, K$, corresponding to K assignments of the driver electrode pair are generated, and for each k, the measurement set $\{f_j^k, j = 1, \ldots, N\}$ is obtained by measuring the voltages at the electrodes. Thus, KN pieces of data $\{(g_j^k = g^k(\partial \mathbf{x}_j), f_j^k),\ j = 1, \ldots, N,\ k = 1, \ldots, K\}$ are collected.

The set of measurements gives ideally (in the limit of many small electrodes and as many measurements) the *Neumann to Dirichlet* mapping: the Dirichlet (u) boundary condition resulting from any Neumann ($\partial u/\partial \mathbf{n}$) condition. The problem we study is to evaluate σ from this mapping. The conductivity depends on the EIT data in a rather weak way. Therefore the inverse problem of EIT is ill-posed.

For simplicity, assume the domain is rectangular $[0, X] \times [0, Y]$, the electrodes are located at the points $(0, y)$, $y = 0, \ldots, Y$, the voltage is predefined on the whole boundary (X, y), and along the other two boundaries assume periodic boundary conditions. Then the following equations are associated with the k-th EIT experiment:

$$\mathcal{L}_\sigma u^k \equiv \nabla \cdot [\sigma(x, y) \nabla u^k(x, y)] = 0, \qquad (x, y) \in \Omega, \tag{1.1}$$

$$\ell_\sigma u^k \equiv \sigma \frac{\partial u^k}{\partial \mathbf{n}}(0, y) = g^k, \tag{1.2}$$

$$u^k(0, y) = f^k. \tag{1.3}$$

This is given for $k = 1, \ldots, K$, the task is to calculate $\sigma(x, y)$ for all $(x, y) \in \Omega$. The data (f, g) usually include errors. The accuracy of measurements is some predefined ϵ.
We assume that the current flux distribution $g^k(y)$ in the domain Ω has a special form

$$g^k(y) = \delta_{J^k}(y), \tag{1.2a}$$

where J^k is the ordinal number of the electrode sending the impulse in the k-th EIT experiment and δ_{J^k} is a δ-function with the impulse at y_{J^k}. Any EIT current flux distribution can be represented as a linear combination of such $g^k(y)$'s. Far from the measurements surface, along (X, y) say, we assume for convenience $u^k(X, y) = 0$ for all y, although in practice a variety of other conditions may be relevant.

Employing local Fourier decompositions, it can be shown [28] that all conductivity-function components of wavelength λ are ill-posed at distances $r \gg \lambda$ from the boundary of measurements. Therefore there is no need to use at such distances fine solution grids. All we can know about the solution can be found with grids whose meshsizes increase proportionality to r. In order to avoid introducing ill-posed components into the current approximation, the changes to the solution far from the measurements should be calculated only on coarse enough grids (with meshsizes at least comparable to the distance from the measurements).

In view of this observation, in the proposed multigrid algorithm a regularization in the classical sense is replaced by a careful choice of grids.

2. Algorithm without explicit regularizaiton

The inverse problem we want to solve is as follows: find an electrical conductivity σ such that equations (1.1)-(1.2) are satisfied and (1.3) is approached as much as possible in the sense of minimizing the "energy" functional

$$E(u^1,\dots,u^K) \stackrel{def}{=} \int_0^Y \sum_{k=1}^K \left[u^k(0,y) - f^k(y)\right]^2 dy. \tag{1.6}$$

2.1. Discretization

Before solving the problem numerically, one should choose a suitable discretization scheme. Consider a finite difference square uniform grid. Let σ be discretized at the grid cell centers, while all other functions are discretized at the grid vertices.

The operator $\mathcal{L}_\sigma$, defined in (1.1), is discretized at grid vertices by second-order discretization. Let us add an exterior "ghost line" of points $(-h, y)$ to the original grid and define the "ghost variables" u and σ as the values of the corresponding functions at the ghost points and ghost cell centers respectively. This allows a central second-order approximation for the operator ℓ_σ, defined in (1.2). In addition, the introduced ghost points enable the extension of the discretization of $\mathcal{L}_\sigma u$ onto the points of $(0, y)$.

For current density distribution (1.2a) the discretization is as follows:

$$g_j^{k,h} = \begin{cases} 1/h, & if\ j = J^k, \\ 0, & otherwise \end{cases}$$

$$j = 1,\dots,N, \qquad k = 1,\dots,K.$$

2.2. Name?

Denote the original (finest) grid of meshsize h_L by G^L. Then introduce the sequence of increasingly coarser grids $G^{L-1}, G^{L-2},\dots,G^1$ of meshsizes $h_{L-1} = 2h_L$, $h_{L-2} = 4h_L,\dots,h_1 = 2^{L-1}h_L$ respectively, such that each coarse grid constitutes the even-numbered rows and columns of the next finer grid.

For each G^l define another set of semi-coarsened grids (or briefly, semi-grids) $G^l = G^l_l$, G^l_{l-1}, $G^l_{l-2},\dots,G^l_1$. The grid G^l_s coincides with four first columns of the grid G^l (parallel to the boundary of measurements), meshsize h_l in x, while in y direction it coincides with the rows of the grid G^s, meshsize h_s, $s = l,\cdots,1$.

FAS

Multigrid

Intergrid communications. The interpolation of an approximation to the coarse grid correction for either u, λ or σ should be of the second order, since this is the highest order of derivatives in the PDE's. We use a bilinear interpolation.

The residuals of all equations are transferred to the coarser levels by full weighting procedure. The coarsening of σ is done also by full weighting. Generally, better restriction of σ is by arithmetic/harmonic averaging as in [15]. However, in the human body σ does not change by orders of magnitude. Therefore the simpler averaging which does not require different

conductivity in the vertical and horizontal directions, is used here. The FAS coarsening of the unknowns u and λ is done by injection.

The FMG interpolation for either u or λ should be at least $p+q$, where p is the order of the discretization and q is the largest order of the difference quotients in the error norms. In our case $p = 2$ and $q = 2$ (if we want the residuals to converge). Therefore we use a cubic FMG interpolation.

The coarsest grid processing. Assume we have a good approximation to σ at all cell centers of the grid. For each such fixed σ the equations for u and λ can easily be solved by Gaussian elimination or any suitable numerical method for solving a linear system, thus yielding (u, λ) as a function of σ. Then we employ the Newton method to solve the equations for σ and to improve the approximation.

Relaxation. It is a most important issue to design a proper relaxation scheme on each grid. First, it is necessarily to identify *the principal terms* of the differential operator on the scale of this grid, then they are relaxed while non-principal terms on that scale are kept unchanged during the relaxation.

2.3. General outline

The algorithm described below is based on three main principles:

1. As a result of a Fourier analysis, we found that the change in the function u at the boundary of measurements, caused by a change in σ that has a form of a local Fourier component, decreases exponentially as a function of the distance r (in meshsizes) from this boundary: $\delta u(0, y) \approx \mathcal{O}(\textit{introduced change} \times \exp^{-Cr/\ell})$, where ℓ is the wavelength of the introduced Fourier component and C is some constant. Hence the computational work on the grid of meshsize h should only be done near the boundary, at distances $\mathrm{O}(h)$ from it.
2. Similar changes introduced into σ at the different $\mathrm{O}(h)$ distances from the boundary of measurements cause *very different* changes in u on this boundary (see figure 1). Thus, for smooth Fourier components in y a full coarsening (both in x and y) does not resolve these differences, hence we must use *a semi coarsening* in the y direction (i.e. without coarsening the meshsize in the x direction).
3. It is necessary to start always from the *better-posed* changes. Therefore, in each cycle (FMG, V-cycle, W-cycle, semi-cycle) we introduce changes to the current approximation first on the coarsest (or semi-coarsest) grid, where those changes are well-posed, and only after that changes from the finer grids.

These considerations gave us the motivation for the following FMG algorithm:

Define a set of the uniform grids G^L, $G^{L-1}, \ldots, G^1$ (as §1.2) of meshsizes h_L, $h_{L-1}, \ldots, h_1$ respectively. For each G^l define another set of semi-coarsened grids (or briefly, semi-grids) $G^l = G^l_l$, G^l_{l-1}, $G^l_{l-2}, \ldots, G^l_1$. The grid G^l_s coincides with four first columns of the grid G^l (parallel to the boundary of measurements), meshsize h_l in x, while in y direction it coincides with the rows of the grid G^s, meshsize h_s, $s = l, \cdots, 1$.

We want to lower the energy functional (1.6). On the grid G^L this functional is discretized as a quadratic function of $u^k_{0,j}$, $j = 1, \ldots, N_L$. $N_l = Y/h_l$, $l = L, \ldots, 1$. The variables of coarser grid G^l interpolated to the finest grid G^L should also minimize this functional. But actually there is no need to interpolate the variables from G^l to G^L. Instead define the

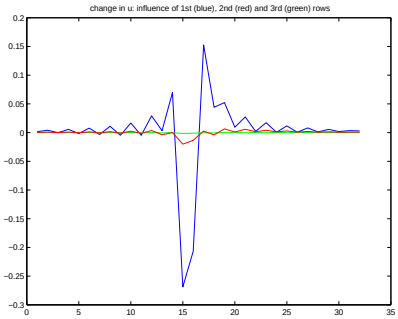

Figure 1. The change in $u(0, y)$ caused by the change in σ at 1st (blue), 2nd (red) and 3rd (green) columns from the boundary of measurements

discrete functional E_L^l as a function of variables $u_{0,j}^k$ on G^l, $j = 1, \ldots, N_l$, as if they *would be interpolated* to the finest grid G^L. Since the interpolation is a linear function of G^l variables, E_L^l is also a quadratic function, which is recursively defined on G^l as follows (using second order interpolation):

$$E_L^l = a_l \sum_{k=1}^{K} \sum_{j=1}^{N_l} {u_{0,j}^k}^2 + b_l \sum_{k=1}^{K} \sum_{j=1}^{N_l} u_{0,j}^k u_{0,j+1}^k + c_l \sum_{k=1}^{K} \sum_{j=1}^{N_l} u_{0,j}^k f_j^k + S_f, \tag{1.7}$$

where $S_f = \sum_{k=1}^{K} \sum_{j=1}^{N_L} {f_j^k}^2$, $(f_j^k)_l = \frac{1}{4}(f_{2j+1}^k)_{l+1} + \frac{1}{2}(f_{2j}^k)_{l+1} + \frac{1}{4}(f_{2j-1}^k)_{l+1}$ and $a_l = \frac{3}{2}a_{l+1} + b_{l+1}$, $b_l = \frac{1}{2}a_{l+1} + b_{l+1}$, $c_l = 2c_{l+1}$ for $l = L-1, \ldots, 1$, $a_L = 1$, $b_L = 0$, $c_L = -2$. Note that inside the semi-cycle (see below for details) the functional $E_L^{l_0}$ translated to the semi-grid $G_l^{l_0}$ yields the same functional E_L^l as in full coarsening ($l = l_0, \ldots, 1$).

Full MultiGrid Cycle:

- Start from the coarsest grid G^1, where all the equations are solved exactly (or nearly exactly), such that σ minimizes the functional E_L^1.
- For $l_0 = 2, \ldots, L$:
  - Interpolate the solution from the grid G^{l_0-1} to the grid G^{l_0} by FMG interpolation.
  - Full-cycle: G^{l_0} is the currently finest grid (see below).

End of Full MultiGrid Cycle.

Full-cycle: G^{l_0} is currently finest grid.

1. For $l = l_0, \ldots, 2$:
   - Semi-cycle: G^l is currently finest grid (see below).
   - Transfer functions u^k and σ from G^l to G^{l-1} by using a *full-coarsening*.

2. On the coarsest grid G^1 solve directly the equations such that σ minimizes E_L^1 (see §3.2 below for details).
3. For $l = 2, \ldots, l_0$:
   - Interpolate the corrections to the functions u^k and σ from G^{l-1} to G^l.
   - Semi-cycle: G^l is currently finest grid (see below).

End of Full-cycle.

Semi-cycle: $G_{l_0}^{l_0} = G^{l_0}$ is currently finest semi-grid.

1. For $l = l_0, \ldots, 2$:
   - Transfer the functions u_k and σ from $G_l^{l_0}$ to $G_{l-1}^{l_0}$ by using *a semi-coarsening*.
2. On the semi-coarsest grid $G_1^{l_0}$ solve the equations exactly, such that σ minimizes E_L^1 (see §3.2 below for details).
3. For $l = 1, \ldots, l_0 - 1$:
   - Interpolate the corrections to the functions u^k and σ from $G_{l-1}^{l_0}$ to $G_l^{l_0}$ by a semi-interpolation procedure.
   - Make a couple of relaxation sweeps: change σ near the boundary of measurements in order to lower E_L^l (see §3.2 below for details).

End of Semi-cycle.

2.4. Changing values of σ

The basic approach is that any change in σ on any grid G^l, $l = 1, \ldots, l$, is designed to minimize the energy functional E_L^l on the currently finest grid G^l, as defined in (1.7)

Assume there exists some approximation to σ on G^l. First, solve the direct problem (1.1)-(1.2) in order to find a function $\vec{u_0}$. Then change the values of σ on a grid G^l by some sufficiently small known δ_0 at m neighboring points according to an appropriate *distributive scheme* (see below for details). Next, find an effect of this change on the grid G^l by local relaxation and find $\vec{u}(\delta_0)$.

The goal is to calculate the change δ that *should have been introduced* to σ on the grid G^l (instead of δ_0), such that the energy functional E_L^l would lower as far as possible. $\vec{u}$ is a function of δ, therefore E_L^l is also a function of δ.

Assume the change in $\vec{u}$ is linearly dependent on δ, i.e.

$$\vec{u}(\delta) = \vec{u_0} + \vec{\alpha}\delta,$$

where $\vec{\alpha}$ is independent of δ and is defined from the calculation with δ_0 by

$$\vec{\alpha} = \frac{\vec{u}(\delta_0) - \vec{u_0}}{\delta_0}.$$

Actually, we do not want the function $E_L^l(\delta)$ to be closer to its minimum than some known ϵ, which is defined according to the accuracy of the measurements and the numerical discretization. Under the above assumption E_L^l is a quadratic function of δ. Its graph is a

parabola in the plane (δ, E). Hence, we have two values for δ correspondingly to the two points of intersection of this parabola and the line $E = \epsilon$. We should choose the smallest δ from those two values, since we are interesting to change an approxiamtion as less as possible with the same change of energy functional. In this way the desired δ is chosen and afterwards is introduced to σ instead of δ_0.

Now let us discuss the *distributive change* in σ, which is a simultaneous change at m neighboring points. For example, change at vertically neighboring points for:
$m = 2$ (1st order distribution):

$$+\delta$$
$$-\delta;$$

$m = 3$ (2nd order distribution):

$$+\delta$$
$$-2\delta$$
$$+\delta.$$

Such a change in σ causes only nearly-local change in u on the same grid. Therefore, it is enough to make just a couple relaxation sweeps for u on fine grids with good enough initial approximation. This drastically decreases the amount of work for re-solving the direct problem there. However, there is no point to apply the distributive change in σ on the coarser grids, since the amount of work for re-solving the direct problem by multigrid cycles there is negligible.

Moreover, since the current density distribution g is as in $(1.2a)$, there is no need to relax u^k for all $k = 1, \ldots, K$. It is enough to relax only those u^k's, for which the impulse of g^k is in the neighborhood, where the change in σ influences.

The important step of the algorithm is an adjustment of the values of the function σ on the coarsest grid G^1 to the currently finest grid G^l, so that the changes in σ on G^1 would lower E_L^1 as far as possible. This process is similar to the one described above, except that the values of σ are changed *simultaneously* at all the G^1 grid points.

3. Numerical results. Work. Conclusions

To perform actual computations for the inverse problem one should first simulate the EIT experiment and to "collect" the appropriate measurement sets. For predefined σ the problem $(1.1) - (1.2)$ is solved and the values of u^k at the boundary of measurements are collected. Some noise is introduced to the data, which are then used by the solver for determining an approximation to σ.

The numerical experiments have been performed for the square domain $[0, 1] \times [0, 1]$. The number of experiments K is equal to the number N of grid points in the y-direction on the finest grid. Then in each experiment k, $g^k(y)$ is a δ-function with an impulse at k. The problem $(1.1) - (1.2)$ has been solved by ten V(1,2)-cycles on the fine grid and the solution at the boundary (0,y) has been transferred by using full weighting to the coarser grids. On the coarsest grid $M = N = 2$.

One problem under consideration was the case when $\sigma(x, y)$ is equal to 2 inside the square $[0, \frac{1}{2}] \times [\frac{1}{2}, 1]$ and 1 elsewhere. The inverse problem with this data may be viewed as representative, since due to ill-posedness, a good approximation to the real σ may be achieved

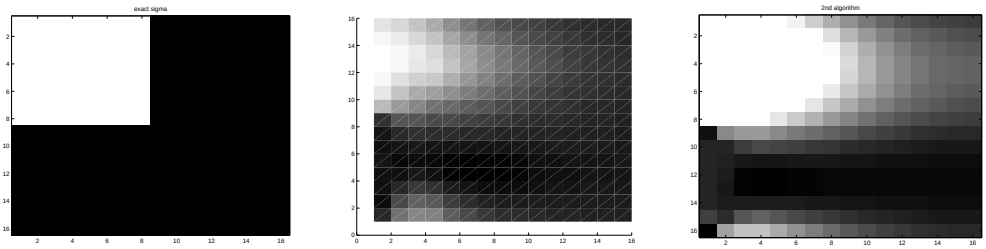

(a) (b) (c)

Figure 2. EIT: (a) exact σ; (b) result of 1st algorithm; (c) result of 2nd algorithm.

only near the boundary of the measurements. σ is discontinuous along this boundary and the accuracy of approximations to such σ there can tell a lot about the correctness of algorithms.

Then this square was moved inside of Ω to a distance of a couple of meshsizes from the boundary of measurements. This inverse problem is in some sense more practical, since EIT is mostly used in order to discover sources inside the domain, while the data are recorded on its boundary. For example, the purpose of EIT for biomedical imaging is to discover tumors in the patient's chest. The conductivity of tumors differs from the conductivity of the healthy tissue. Such tumors are usually located deep inside the body, while electrodes are attached to the chest. The same situation is true also for EIT in other areas (geophysical, for instance).

In the algorithm with grid regularization the distributive change of first order in the vertical direction (with overlaps) at two columns near the boundary of measurements was introduced to σ on the finest and on the next to the finest levels.

Both algorithms approximate very well the behaviour of σ near the boundary of measurements and less well when moving deeper into domain (as would be expected from the ill-posed type of this problem).

The accuracy of both algorithm, in particular near the boundary of measurements, is nearly the same. But the algorithm described in §3 does not use any regularization in a classical sense, and as a result significant space and time saving is achieved. In this algorithm there is no need to solve a large system of discretized differential equations and boundary conditions; also, no Lagrange-multiplier equations need to be treated.

At this point we still spend quite a lot work to calculate repeatedly changes of the functional (1.7) due to changes in $u^k(0, y)$ at a small neighborhood of each relaxation step. The sum in (1.7) includes all K terms, while actually most of those terms have really a negligable contribution to the change of this functional at each step of relaxation. Therefore, we suggest to reduce the amount of work by taking into account at each step only terms k for which the electrode J^k (see (1.2a)) is close to the relaxation neighborhood.

The amount of work for solving the inverse problem for EIT is expected to be proportional to the number of points on the boundary of measurements only (in our formulation Work $\sim CN$ if $N = M = K$, C is some large constant). It illustrates that solving an inverse problem can even be cheaper than solving the corresponding direct problem, when the nature of ill-posedness is well-understood.

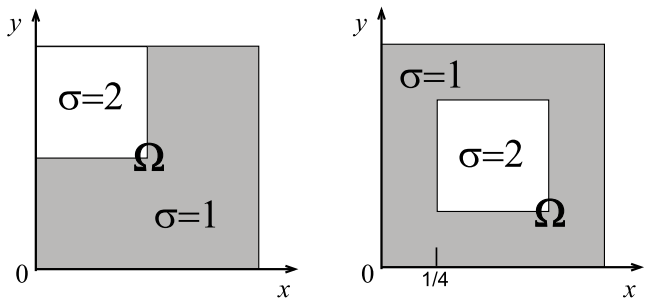

Figure 2.6. EIT: white region represents the "tumor" placement. Two domains used in the experiments.

REFERENCES

1. R. E. Alcouffe, A. Brandt, J. E. Dendy, J. W. Painter, *The multigrid method for the diffusion equation with strongly discontinuous coefficients*, SIAM J. Sci. Stat. Comput., 4 (1981), vol. 2, pp. 430–454.
2. G. Alessandrini, *Stable determination of conductivity by boundary measurements*, Applicable analysis, 27 (1988), pp. 153–172.
3. U.M. Ascher, E. Haber, *Grid refinement and scaling for distributed parameter estimation problems*, Inverse problems, 17:571-590, 2001.
4. A. Brandt, *Multigrid solvers for non-elliptic and singular-perturbation steady-state problems*, the Weizmann Institute of Science, 1981.
5. A. Brandt, *1984 Multigrid Guide with Applications to Fluid Dynamics,* GMD-Studie 85, St. Augustin, 1985.
6. A. Brandt, *Multiscale Scientific Computation: Review 2001*, Lecture notes in comp. science and eng., 20 (2002), 3-95, Springer.
7. A. Brandt, *Rigorous quantitative analysis of multigrid: I. Constant coefficients two level cycle with L_2 norm*, SIAM J. Numer. Anal. 31 (1994) 1695-1730.
8. A. Calderon, *On an inverse boundary value problem*, Seminar on Numerical Analysis and its Applications (W. Meyer and M. Raupp, eds.), Brazilian Mathematical Society, Rio de Janeiro, 1980, pp. 1–7.
9. P. C. Franzone, *Some inverse problems in electrocardiology*, Numerical Treatment of Inverse Problems in Differential and Integral Equations (P. Deuflhard and E. Hairer, eds.), Birkhäuser, 1983.
10. R. Gandlin, *Multigrid Algorithms for an Inverse Problem in Impedance Tomography*, M. Sc. thesis, the Weizmann Institute of Science, 1998.
11. R. Gandlin, *Multigrid Solvers for some Inverse Problems,* Proposal for Ph.D. Thesis, Weizmann Institute of Science, 1999.
12. R. Gandlin, *Multigrid Solvers for some Inverse Problems*, Intermediate report, Weizmann Institute of Science, 2000.
13. P. Kohn and M. Vogelius, *Determining conductivity by boundary measurements*, Comm. Pure Appl. Math., 37 (1984), pp. 289–298.
14. V. A. Morozov, *Methods for Solving Incorrectly Posed Problems,* Springer-Verlag, 1984.
15. F. Shmulyian, *Multigrid Algorithms for an Inverse Problem in Impedance Tomography*, M. Sc. thesis, the Weizmann Institute of Science, 1995.
16. J. Sylvester and G. Uhlmann, *A global uniqueness theorem for an inverse boundary value problem*, Annals of Math., 125 (1987), pp. 153–169.
17. L. Borcea, *Electrical Impedance Tomography*, Inverse Problems, 18, No. 6, 2002, pp. R99-R136.
18. D. Isaacson, M. Cheney, *Effects of measurement precision and finite number of electrode on linear impedance imaging algorithms*, SIAM J. Appl. Math., pp. 1705-1731, 1991.
19. A. Allers, F. Santosa, *Stability and resolution analysis of a linearized problem in electrical impedance tomography*, Inverse problems, 7:515-533, 1991.
20. D.G. Gisser, D. Isaacson, J.C. Newell, *Electric current computed tomography and eigehnvalues*, SIAM J. Appl. Math., 50(6): 1623-1624, 1990.

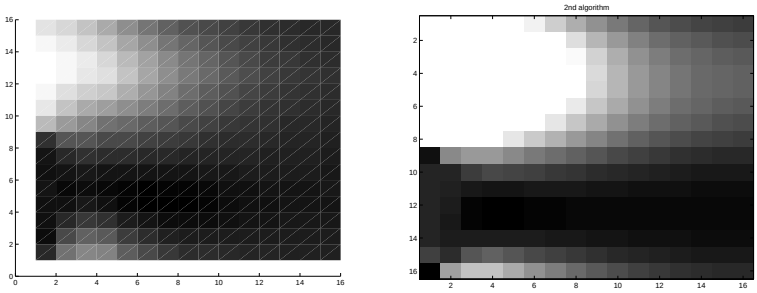

(a) (b)

Figure 2.7. Result of (a) 1st algorithm with small regularization; (b) 2nd algorithm for domain shown on fig. 2.6a.

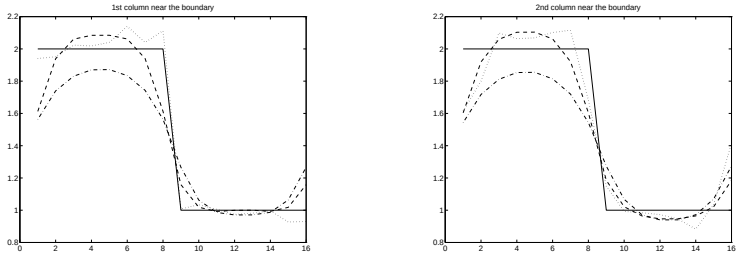

(a) (b)

Figure 2.8. Results of the algorithms for cases shown on fig. 2.6a: (a) 1st column, (b) 2nd column near the boundary $x = 0$

– exact σ, $-\cdot-$ 1st algorithm with large regularization
$--$ 1st algorithm with small regularization, $\cdots$ 2nd algorithm.
Note: periodic boundary conditions.

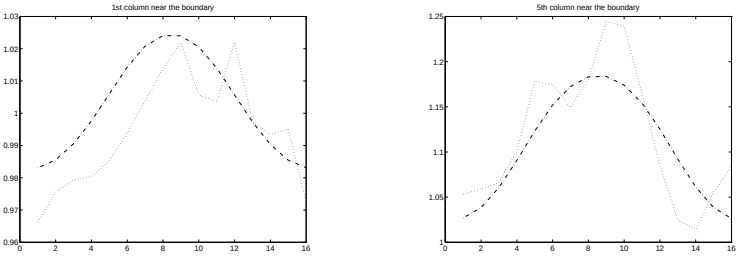

(c) (d)

Figure 2.9. Results of the algorithms for cases shown on fig. 2.6b: (c) 1st column near the boundary, (d) column at $x = 1/4$.

– 1st algorithm with small regularization, $-\cdot-$ 2nd algorithm .

21. E. Cherkaeva, A. Tripp, *Inverse conductivity problem for noisy measurements*, Inverse problems, 12:869-883, 1996.
22. D. Barber, B. Brown, *Recent developments in applied potential tomography*, in Amsterdam S. Bacharach ed., Nijhoff ed., Information processing in medical imaging, pp. 106-121, 1986.
23. M. Cheney, D. Isaacson, J.C. Newell, *Electrical impedance tomography*, SIAM review, 41(1):85-101, 1999.
24. H.W. Engl, M. Hanke, A. Neubauer, *Regularization of inverse problems*, Kluwer Academic Publishers, Dodrecht, 1996.
25. S.F. McCormick, J.G. Wade, *Multigrid solution of a linearized regularized least-squares problem in electrical impedance tomography*, Inverse problems, 9:697-713, 1993.
26. L. Borcea, *A nonlinear multigrid for imaging electrical conductivity and permittivity at low frequency*, Inverse problems, 17(2):329-359, 2001.
27. R. Gandlin, *Multigrid Solvers for Inverse Problems,* Ph.D. Thesis, Weizmann Institute of Science, 2003.
28. S. Agmon, A. Douglis, L. Nirenberg, *Estimates near the boundary for solutions of elliptic partial differential equations satisfying general boundary conditions, I and II,* Comm. Pure Appl. Math., vol. 12, 623-727, 1959.